Smart Structures and Systems, *Vol. 30, No. 3 (2022) 255-261*
https://doi.org/10.12989/sss.2022.30.3.255

Experimental characterization of a smart material via DIC

Sara Casciati*[1], Daniele Bortoluzzi [1a], Lucia Faravelli [1b] and Luca Rosadini [2c]

[1] *SIART Srl, via dei Mille 73, Pavia, Italy*
[2] *Formerly SIART Srl, via dei Mille 73, Pavia, Italy*

(*Received June 10, 2022, Revised July 17, 2022, Accepted July 17, 2022*)

Abstract. When no extensometer is available in a generic tensile-compression test carried out by a universal testing machine (for instance the model BIONIX from Material Testing Systems (MTS)), the test results only provide the relative displacement between the machine grips. The test does not provide any information on the local behaviour of the material. This contribution presents the potential of an application of Digital Image Correlation (DIC) toward the reconstruction of the behaviour along the specimen. In particular, the authors test a Ni-Ti shape memory alloys (SMA) specimen with emphasis on the coupling of the two measurement techniques.

Keywords: data collection; digital image correlation; shape memory alloy; universal testing machine; vision-based techniques

1. Introduction

Vision-based techniques had an impressive development in the last five years (Hu *et al*. 2019, 2021, Kang *et al*. 2021). Since the International Conference on Digital Image Correlation and Noncontact Experimental Mechanics (IDICS2018), held in Hangzhou on October 2018, (Casciati *et al*. 2019), there is no issue of the relevant specialized scientific journals that does not contain at least one paper exploiting vision-based tools.

This technique employs tracking and image registration techniques for accurate measurements of changes in images in order to measure full-field displacements and strains in many areas of science and engineering. When compared to standard measurement approaches (e.g., strain gages and extensometers), this method may count in a wider amount of information gathered thanks to the ability to provide both local and average data via Digital Image Correlation (DIC). Digital Image Correlation (DIC) is a non-contact and non-interferometric optical method used for measuring the displacement and deformation of a structural element or material subjected to external actions. One needs one or more than one digital cameras to capture consecutive images (photos/pictures) of the surface of a tested object/material, before and during the deformation period, along with dedicated computer software and algorithms recreate a set of displacement/deformation maps for the entire specimen surface. The method is based on mathematical correlation analysis. Commonly, DIC relies on finding the maximum of the correlation array between pixel-intensity array subsets on two or more corresponding images. This gives the integer translational shift between them. It is also possible to estimate shifts to a resolution finer than the resolution of the original images, which is often called "subpixel" registration. Finally, an iterative approach could be used to maximize the interpolated correlation coefficient by using nonlinear optimization techniques.

The early stage of this research activity focused attention on the ability to catch dynamic phenomena (Wu *et al*. 2014). Further implementations of the technique were addressed to real applications such as the realization of a "simple and rapid" structural monitoring of buildings subjected to external source of vibrations (e.g., during the excavation phase). In particular, this was the topic addressed, within the Horizon2020 EU project GEOFIT, by its deliverable D2.6 "Displacement Based Monitoring Methodology" available on-line.

The main limitations to overcome in these dynamic applications were:

1. the technological limitation of the collection rate, in terms of frame per second, of the available vision devices and
2. the huge dimension of the information to be stored.

Recently the interest moved toward quasi-static phenomena, mainly those that the operator can directly control as tests carried out in laboratory (Rosadini 2019).

The authors investigate in this paper the feasibility of applying a vision-based displacement-measurement technique in the characterization of a Ni-Ti shape memory alloy (SMA) frequently proposed in the literature for being exploited within damper devices (Zheng *et al*. 2019, Qiu *et al*. 2020). Previous experimental campaigns addressed the characterization of the damper as a whole (Wang *et al*.

*Corresponding author, Ph.D.,
E-mail: sara@dipmec.it
[a] Ph.D.
[b] Professor
[c] Engineer

ISSN: 1738-1584 (Print), 1738-1991 (Online)

2020, 2021). Here the focus is on the material. It is worth noticing that the vision equipment itself is a simple smartphone as offered by the market.

2. Experimental mock-up and test description

The experimental test campaign adopts a BIONIX machine produced by the company "Material Testing Systems" (MTS). Provided the specimen can be gripped, the machine is able to stretch any metallic and non-metallic specimen by a sequence of tensile and compressive forces of predefined values. A computer controls the behavior of the MTS machine, with the software able to drive several kinds of tests on the specimen.

A commercial smartphone collects images for successive elaboration via Digital Image Correlation (DIC). The image acquisition speed reaches 10 frames per second, but this aspect will be discussed in next section.

The sensors built in the MTS machine supplies information about the extremes of the specimen. Digital image correlation addresses the central area of the specimens.

A system of LED (light-emitting diode) markers is glued on the MTS machine grips, as well as along the alloy specimens. Two different sizes of markers are compared, each with the other, in view of ensuring the richest collection of bits of information on the alloy behaviour.

The alloy specimens were obtained from the U-shaped dampers widely discussed in Casciati *et al*. (2019), Wang *et al*. (2020, 2021). In order to obtain an item consistent with the test specifications, the damper element was cut into a plane rectangular specimens, preserving the two existing circular holes as shown in Fig. 1.

Using special grips with a tightening of 14 MPa, the SMA specimen was mounted on the MTS machine. Only one of the two circles in Fig. 1 is left between the two grips (Fig. 2). Therefore, the resulting specimen geometry is that in Fig. 3.

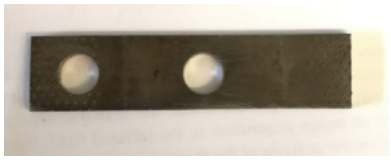

Fig. 1 The specimen of the considered metallic alloy

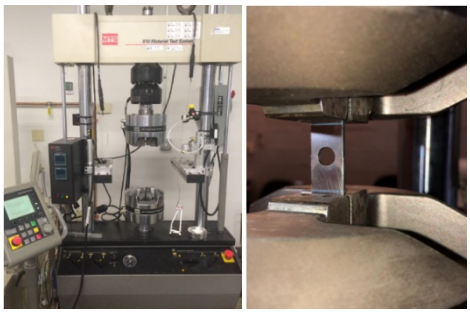

Fig. 2 The used MTS machine (left) with the SMA specimen mounted on the grips (right)

The thickness is 0.2 cm, i.e., the section area is 30 mm^2 in the zones not including the circle, while goes down to 14 mm^2 at the location of the center of the circle.

The developments of next sections require first a rough estimate of the effects of the testing conditions on the results. The MTS machine software system directly collects data from the lodged sensors, which immediately supply the results of the test carried out. One focuses on the axial force N and the elongation Δl as reported in Fig. 4.

This preliminary test shows some features that will be preserved in all the tests reported in next sections. Namely, along the loading stage, one adopts the displacement control mode. In order not to compress the specimen, the descent path adopts the force control mode (not the displacement control as for the ascending branch).

This choice has three main consequences:

a) The descent path is not linear in the time-displacement plot given at the top of Fig. 4;
b) At the peak value, one detects in the force-displacement plot, given in the bottom of Fig. 4,

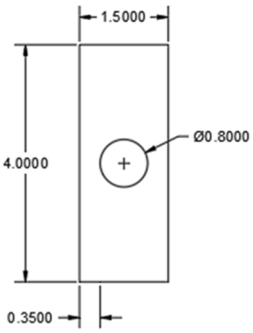

Fig. 3 Specimen geometry [lengths in *cm*]

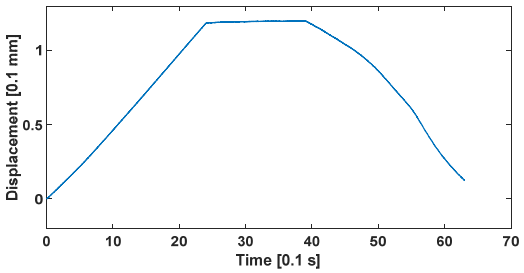

(a)

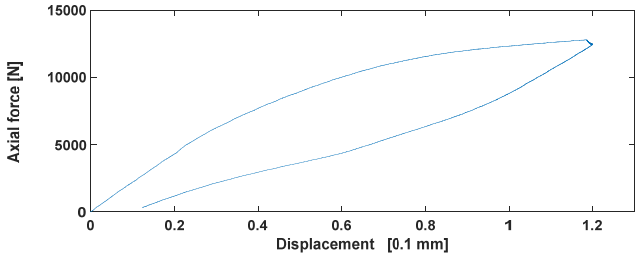

(b)

Fig. 4 Single cycle test as detected by the testing machine sensors: (a) time-displacement plot; (b) displacement-stress plot

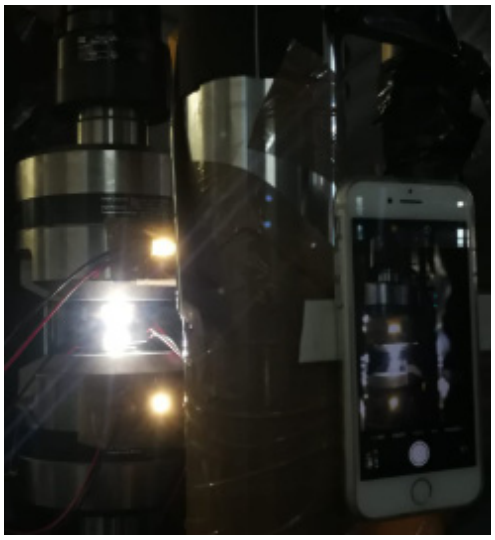

Fig. 5 Four markers are glued on the machine-specimen system

Fig. 6 Video progress for checking the actual frames per second rate: (a) images 1 and 5; (b) image 9

a jump;

c) The final displacement corresponds to a zero force but it is greater than zero.

Each of the successive tests carried out lasts less than ten seconds. The time window is divided as follows:

a) the shape memory specimen is loaded up to a total displacement of length of 1.2 millimetres. The test proceeds at the speed of 0.5 mm/s for 2.4 seconds.
b) a pause of the duration of 1.4 seconds follows. This because the ascent path has not to influence the descent path. This interval allows the specimen to stabilize in the deformed configuration; the control mode is shifted from displacement to force;
c) the computer drives back the specimen to the zero force status, different from the initial conditions. The duration of this last step is still 2.4 seconds.

3. Implementing the DIC

3.1 Using markers

As far as digital image is concerned, in order to obtain optimal results, it is advisable to implement some tricks to drive the elaborations. In this case, LED markers are used to identify the points of interest of the system, consisting of both MTS machine and SMA specimen. In particular, four markers are glued as shown in Fig. 5:

i) the first marker is placed on the area of the MTS machine supporting the bottom grip. It remains at rest during the entire test;
ii) two LEDs are glued on the SMA profile, one above and the other below the hole.
iii) the fourth LED marker is set on the mobile part of the MTS machine, i.e., the upper grip.

Two reference markers are usually added. A screen located beyond the test area hosts them. They remain at rest during all the duration, providing an absolute reference system.

3.2 Camera mode

The images are acquired by a smartphone. One has to guarantee the perpendicularity between the object investigated and the camera. Therefore, the iPhone 8 is fixed on a specially designed support.

When operating the camera of a smartphone, one has several options. That appearing more suitable is the video mode. For it the frames-per-second rate can be set as 24, 30 or 60. Fig. 6 summarizes the validation test carried out by the authors. It comes with images from a video of a second phone screen when a chronometric application was running. In Fig. 6(a) images 1 and 5 are shown: the time step is 0.04275 s and the frame rate nearly 24; Fig. 6(b) shows the ninth image with a global time step of 0.043. In conclusion, the rate of acquisition is not very stable for scientific applications purposes. However, the main drawback preventing from using the video mode is that, in view of the elaborations listed in the next sub-section, one needs to edit the images after having unbundled them.

This suggested to use the policy adopted in (Casciati *et al*. 2019): pushing the button with continuity produces a sequence of images spaced of 0.1 s and the frame rate was found quite stable on the iPhone 8. The format of each image is the standard “jpg”. It is worth noticing that smartphones coming from different producers come with different rates and its value was not so stable as in the used device.

3.3 Images editing

A direct use of the collected images in the software introduced in next sub-section would not allow one to reach the expected results.

Fig. 7 Assigning the AoI to the elaboration software

Each single image covers a broad area, much wider than that where the markers are located. A better performance of the elaboration software is obtained by assigning an Area of Interest (AoI) as shown in Fig. 7. Moreover, this figure shows a very dark photo that is obtained by editing the single image in the sequence by removing brightness.

The contrast of the image is set in such a way that only bright pixels emerge from the background. The software for such editing stage acts on a single image in the "jpg" format and this supports the choice, of previous sub-section, of operating the camera in the photo mode.

3.4 Images elaboration

After the images collection by a hardware and their editing by a suitable general-purpose software, one needs a specialty software (i.e., Image-Pro Plus) able to calculate the displacements using image-processing algorithms and coordinate transformations. The achieved estimates of the motion are based on the pixels. Once one knows the conversion factor between pixels and millimetres and a reference coordinate system is selected, standard displacement time histories are obtained. The conversion ratio between pixel and millimetre is 0,305 given by the ration among the LED's distance [mm] and the related distance expressed in pixel. Note that the number of images in the sequence strongly affects the number of MB one needs for the storage.

The unusual aspect is that the software automatically detects the luminous points (markers) to be followed across the images sequence.

Reflection and refraction phenomena could result in unwished fictitious targets that must be ignored in future elaboration. Fig. 8 comes with a comparison of an image taken in the ascent phase with one in the descent phase, after the change in the testing machine mode control. In the former case, 11 tracers are detected by the software, while in the second case one only finds the expected 6 (4 plus the 2 of reference). This is summarized in Fig. 8. The different number of detected tracers is the result of different light exposition in the two tests.

To help the reader in reading Fig. 8, one observes on the

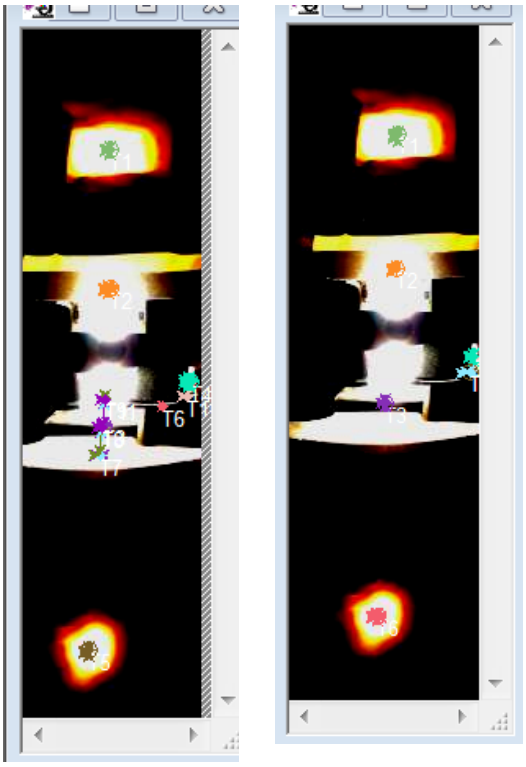

Fig. 8 Tracers in the ascent (left) and in descent (right) phases as identified from the elaboration software. The tracers are directly identified by the software

clean image on the right side the tracers T1, T2 and T3 from the top toward the bottom. Then T4 and T5 label the reference markers and T6 is the marker on the machine grip at rest. In the image on the left, this last marker is denoted as T5, the first two markers are well identified, while there is a flicker of lights around the position of T3.

4. Test results

A first sequence of tests was carried out by adopting rather wide markers, as suggested by the need of making the desired points visible. The results of the loading stage are given in Fig. 9. The variability of the points around the expected backbone (mainly for the bottom marker supposed to remain at rest) suggested to adopt markers of smaller diameter (3 mm diameter the smaller ones, versus 5 mm diameter the bigger ones). The resulting higher accuracy is kept in Fig. 10.

The following remarks apply:

1. The lower marker in Fig. 10 (T4) shows the expected behaviour: it remains at rest for the duration of the single stages of the test. The jump in the middle is generated when the machine operator moves to the force control mode from the initial displacement control mode.
2. The curve associated with the top marker (T1) shows a satisfactory agreement with the solid line curve which represents the data recorded by the sensors built in the universal testing machine.

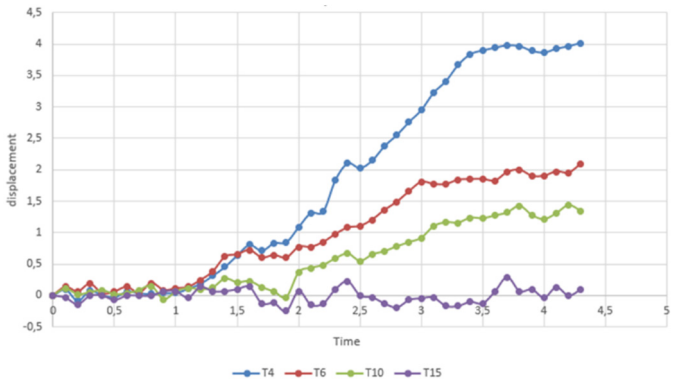

Fig. 9 Displacement (pixels) versus time (in 0.1 second) during the loading stage as detected by using large markers. T4 (blue) top marker; T6 (red) and T10 (green) middle markers; T15 (purple) bottom marker

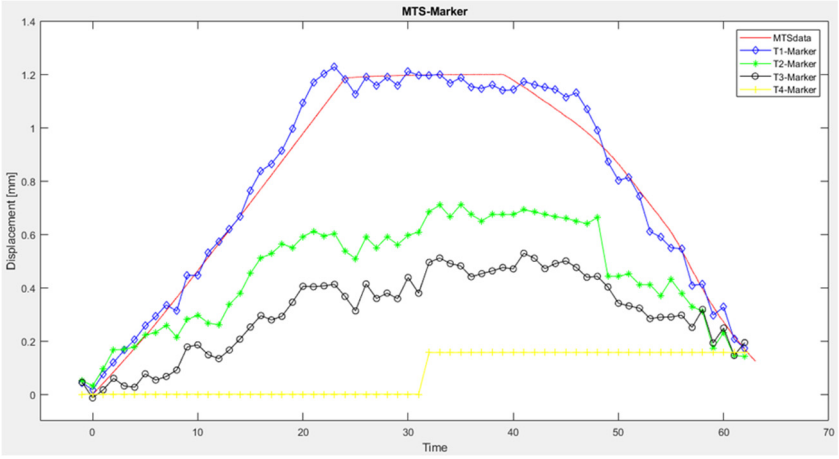

Fig. 10 Displacement (in 0.1 mm) versus time (in 0.1 second) during the loading stage as detected by using small markers. The curve at the top of Figure 4 is also included for sake of comparison

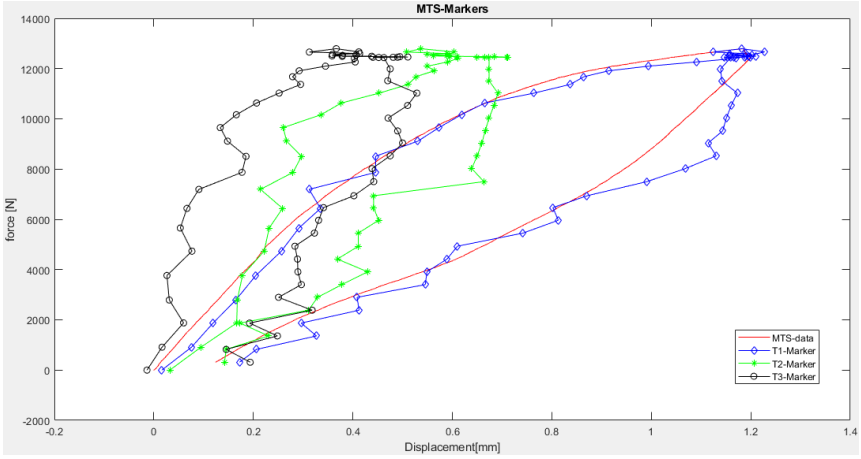

Fig. 11 Force (in N) versus displacement (in 0.1 mm) during the loading-unloading cycle as detected by using small markers. The curve at the bottom of Figure 4 is also included for sake of comparison

3. The marker T2 is located below the hole in Fig. 3. The curve associated with this marker shows a nearly linear behaviour of the elongation of the specimen part below. This is consistent with the compactness of that part of the specimen.
4. The marker T3 is located above the hole in Fig. 3. The curve associated with this marker starts steeply, but soon the occurrence of local phenomena is outlined.
5. Both the curves associated with the markers T1 and

T2 show in the descending path the jump typical of the constitutive law of shape memory alloys.

Fig. 11 is the final original innovative contribution of this paper. The three loops give the differences between the three hysteretic responses of the three parts of the specimen.

a) The line on the left depends on the full rectangular section of 30 mm^2;
b) the line in the middle accounts for the reduction of section from 30 to 14 mm^2 and then again up to 30 mm^2;
c) the line on the right, to be compared with that caught by the testing machine provides the response of the whole specimen.

The first interesting consideration covers the change from the displacement control mode to the force control mode. The effects are detected when the displacement is at its maximum value. It is evident how the influence is nearly negligible for the marker T1 mounted on the upper grip, while it is quite effective on the intermediate markers T2 and T3.

A second remark sees the confirmation of the jumps at the beginning of the descent paths in the curves associated with the markers T1 and T2.

On the basis of the two above remarks, one can comment the hysteresis loops:

- the curve associated with the marker below the hole (T3) does not show an actual hysteresis. Indeed, the change of control mode causes here as in T4 a significant jump in the displacement value. The result is that the ascent and descent paths appear as parallel lines, their distance being the value of the residual displacement;
- the curve associated with the marker T2 shows the expected hysteretic shape;
- the curve of the marker T1 shows the corrected shape, but the extent of the displacement maximum value, when compared with that of the marker T2, is quite large and denote that the progressive reduction of the Young's modulus of the alloy as the stress increase also spreads in the upper part of the specimen.

5. Conclusions

This paper moves from the results in (Casciati *et al*. 2019) where the performance of camera devices was compared by testing a U-shaped shape memory alloy damper. The attention there was on the possibility to catch the dynamic response of the damper.

The development implemented here focuses the attention on the quasi-static response of a shape-memory-alloy specimen. In this context, the camera of a smartphone is used toward the acquisition of data that in standard laboratory testing would requires the use of one or more extensometers (usually quite bulky and not of easy installation on small specimens).

The specimen was selected to have a variable section and the adopted vision based technique was able to outline the different responses of the different parts of the specimen. As outlined above, when the specimen was introduced, it preserves a rather wide hole in it. This allows one to conceive an experiment with quite different contributions to the global response from the single transverse stripes of the specimen. The goal was to detect these differences by a vision based technique; it was successfully accomplished.

While in this manuscript the DIC potential is investigated by adopting a quite special material specimen, allowing one to detect different response along it, future developments should afford the task of a simultaneous use of DIC and strain gauges. The task is not of easy solution, due to the conflictual size of the latter with the DIC markers.

Future research effort should address two aspects:

1) the possibility of introducing smoothing techniques to cancel the sharpness in the plot presently returned by the software for the elaboration of images;
2) the main drawback one encounters when dealing with vision-based tools: the huge amount of data storage required even for test of short duration.

Techniques of data reduction are in development and could greatly facilitate the adoption of vision-based techniques in structural monitoring.

Acknowledgments

The activity reported in this paper has received funding from the *European Union Horizon 2020* research and innovation program under grant agreement **No. 792210** (GEOFIT).

References

Casciati, F., Casciati, S., Colnaghi, A., Faravelli, L., Rosadini, L. and Zhu, S. (2019), "Vision-based support in the characterization of superelastic U-shaped SMA elements", *Smart Struct. Syst., Int. J.*, **24**(5), 641-648. https://doi.org/10.12989/sss.2019.24.5.641

GEOFIT, https://geofit-project.eu/publications-and-results/project-deliverables/

Hu, Y., Sun, X., Zhu, W. and Li, H. (2019), "Local damage detection of a fan blade under ambient excitation by three-dimensional digital image correlation", *Smart Struct. Syst., Int. J.*, **24**(5), 597-606. https://doi.org/10.12989/sss.2019.24.5.597

Hu, Y.D., Xia, Q., Hou, R.R., Xia, Y. and Yan, J.Y. (2021), "Computer vision-based displacement measurement with m-sequence target", *Smart Struct. Syst., Int. J.*, **27**(3), 537-546. https://doi.org/10.12989/sss.2021.27.3.537

Kang, M.S., Im, S.B. and An, Y.-K. (2021), "Evaluation of crack opening phenomenon using subset-optimized digital image correlation", *Smart Struct. Syst., Int. J.*, **27**(5), 761-768. https://doi.org/10.12989/sss.2021.27.5.761

Qiu, C., Gong, Z., Peng, C. and Li, H. (2020), "Seismic vibration control of an innovative self-centering damper using confined SMA core", *Smart Struct. Syst., Int. J.*, **25**(2), 241-254. https://doi.org/10.12989/sss.2020.25.2.241

Rosadini, L. (2019), "Digital Image Correlation" (DIC) come base per il monitoraggio strutturale "vision based" (in Italian), University of Pavia, Master Thesis in Civil Engineering.

Wang, B., Zhu, S. and Casciati, F. (2020), "Experimental study of novel self-centering seismic base isolators incorporating superelastic shape memory alloys", *J. Struct. Eng. ASCE*, 04020129. https://doi.org/10.1061/(ASCE)ST.1943-541X.0002679

Wang, B., Zhu, S., Casciati, F., Chen, K. and Jiang, H. (2021), "Cyclic behavior and deformation mechanism of superelastic SMA U-shaped dampers under in-plane and out-of-plane loadings", *Smart Mater. Struct.*, **30**, 055009. https://doi.org/10.1088/1361-665X/abedf4

Wu, L.J., Casciati, F. and Casciati, S. (2014), "Dynamic testing of a laboratory model via vision-based sensing", *Eng. Struct.*, **60**, 113-125. https://doi.org/10.1016/j.engstruct.2013.12.002

Zheng, Y., Dong, Y., Che, B. and Anwar, G.A. (2019), "Seismic damage mitigation of bridges with self-adaptive SMA-cable-based bearings", *Smart Struct. Syst., Int. J.*, **24**(1), 127-139. https://doi.org/10.12989/sss.2019.24.1.127